

Article

An Assessment of Zeolite Framework Effect for Low-Temperature NO_x Adsorbers

Lidia Castoldi ^{1,*}, Sara Morandi ^{2,*}, Pierfrancesco Ticali ², Roberto Matarrese ¹ and Luca Lietti ¹

¹ Laboratory of Catalysis and Catalytic Processes, Department of Energy, Politecnico di Milano, Via La Masa 34, 20156 Milano, Italy; roberto.matarrese@polimi.it (R.M.); luca.lietti@polimi.it (L.L.)

² Department of Chemistry, NIS Center and INSTM Reference Center, Università di Torino, Via P. Giuria 7, 10125 Torino, Italy; pierfrancesco.ticali@unito.it

* Correspondence: lidia.castoldi@polimi.it (L.C.); sara.morandi@unito.it (S.M.); Tel.: +39-0223993255 (L.C.); +39-0116707539 (S.M.)

Abstract: Pd-promoted zeolites (Y, ZSM-5, FER, SSZ-13) were prepared and characterized to analyze their properties as low-temperature NO_x adsorbers. The samples were investigated by BET and XRD and by in situ FT-IR spectroscopy of CO and NO adsorption to probe the Pd sites and the nature of the adsorbed NO_x species. The NO_x adsorption/desorption performances at low temperatures were examined by microreactor measurements upon NO/O₂ adsorption followed by TPD in the presence of water and carbon dioxide. It was enlightened that: (i) the zeolite framework influences the Pd dispersion: the smaller the zeolite cage, the higher the Pd dispersion, irrespective of the Si/Al ratio. Accordingly, the following Pd dispersion order has been observed, inversely to the zeolite cage size: Pd/SSZ-13 > Pd/ZSM-5 ~ Pd/FER >> Pd/Y; (ii) Pd is present as isolated Pdⁿ⁺ species and in PdO_x particles; (iii) the Pd dispersion governs the NO_x storage capacity: the smaller the zeolite cage, the higher the Pd dispersion and the storage capacity; (iv) NO adsorbs mainly in the form of Pd nitrosyls and nitrates; (v) NO desorption occurs both at a temperature below 200 °C and in a high-temperature range (near 350 °C).

Keywords: PNA; Pd-zeolites; NO_x; nitrosyls; low temperature adsorption; FT-IR spectroscopy



Citation: Castoldi, L.; Morandi, S.; Ticali, P.; Matarrese, R.; Lietti, L. An Assessment of Zeolite Framework Effect for Low-Temperature NO_x Adsorbers. *Catalysts* **2023**, *13*, 962. <https://doi.org/10.3390/catal13060962>

Academic Editors: Giuseppe Pantaleo and Leonarda Liotta

Received: 30 April 2023

Revised: 28 May 2023

Accepted: 30 May 2023

Published: 1 June 2023



Copyright: © 2023 by the authors. Licensee MDPI, Basel, Switzerland. This article is an open access article distributed under the terms and conditions of the Creative Commons Attribution (CC BY) license (<https://creativecommons.org/licenses/by/4.0/>).

1. Introduction

The severe NO_x emission regulations enforced in the automotive sector [1] call for highly efficient NO_x reduction techniques. Currently adopted technologies for lean-burn engines are the NO_x-storage reduction (NSR) technique, also referred to as Lean NO_x traps (LNT) [2,3], and the urea selective catalytic reduction (SCR) [4]. In fact, both techniques are not efficient for the reduction in NO_x emissions at low temperatures, as required by recent regulations, especially for hybrid vehicles where the endothermic engine is continuously subjected to start and stop cycles [5,6].

The use of passive NO_x adsorber (PNA) systems installed upstream of the SCR or LNT systems has been recently proposed to mitigate cold-start NO_x emissions. In this configuration, PNAs store NO_x at low temperatures; the trapped NO_x are then released at higher temperatures when the NO_x reduction catalysts placed downstream effectively accomplish the NO_x abatement [7–10].

In 2016, Johnson Matthey [11] reported a very efficient formulation for PNA systems based on acidic zeolites doped with Pd. In that work, the authors compared the behavior of different zeolite structures, including MFI (Mobil-type five), CHA (chabasite), and BEA (Beta). These systems showed remarkable NO_x storage capacity at 100 °C, with release of the trapped NO_x at a temperature suitable for practical application, i.e., near 200 °C. It was found that the framework structure of the zeolites affects the NO_x storage capacity and the desorption temperature; in particular, the authors pointed out that at 100 °C the

zeolites with the largest pore size exhibit the highest storage capacity, and the lowest NO_x desorption temperature during heating.

Starting from this pioneering work, research on zeolite-based LTNAs has intensified in recent years [12–17]. Zheng et al. [13] compared Pd-doped ZSM-5 (Zeolite Socony Mobil-type 5) and SSZ-13 (framework type code CHA) zeolites, finding out that in these materials Pd is present as atomically dispersed species in the cationic sites of the zeolite, and as PdO_x particles on the external surfaces. In particular, it was reported that while Pd is largely dispersed in ZSM-5, the small pore opening of SSZ-13 inhibits Pd diffusion, favoring the formation of PdO_x particles on the external surfaces. Lee et al. [16] also showed differences in the Pd mobility within ZSM-5 and SSZ-13: during oxidative and hydrothermal treatments, the smaller pore size of SSZ-13 contributed to the lower Pd mobility with respect to ZSM-5. Along similar lines, Pace et al. [17] compared Beta and CHA zeolites, finding that these materials show different distributions of Pd species. Notably, it is generally agreed that Pd loadings near 1 wt% lead to the formation of isolated Pd ions, which are recognized as active sites for low-temperature NO_x storage [18–21].

The literature survey points out the extreme complexity of these systems as the nature of Pd surface sites is influenced by many factors, including the zeolite structure. Aiming at a better understanding of how the morphological characteristic of the zeolite affects the nature of the Pd sites and their involvement in the NO_x storage, in this study, a large-pore zeolite (Y-zeolite, with Faujasite FAU structure), two medium-pore zeolites (ZSM-5, with MFI structure, and Ferrierite FER), and a small-pore zeolite (SSZ-13, with CHA structure) have been considered. These zeolites have been doped with Pd, and the effect of the zeolite framework on the NO_x adsorption/desorption performances has been investigated. In particular, NO_x adsorption and desorption experiments under simulated exhaust conditions (i.e., in the presence of both H₂O and CO₂) have been performed, along with in situ FT-IR spectroscopy studies to point out the NO_x adsorption activity/nature of the zeolite substrate relationships. The effect of the Si/Al ratio on the sample performances could also be considered in that zeolites with the same pore size but different Si/Al ratios (FER and ZSM-5) have been considered and compared.

2. Results and Discussion

2.1. Sample Characterization

2.1.1. Structural and Morphological Characterization

Y zeolite exhibits the Faujasite (FAU) framework; it is a large-pore zeolite (pore openings of 7.4 Å), and its structure contains a 3D pore system limited by 12-member rings. Ferrierite (FER framework) and ZSM-5 (MFI framework) are medium-pore zeolites whose structure contains a 2D system of intersecting pores limited by 8- and 10-member rings for FER and 10-member rings for ZSM-5. SSZ-13 is a small-pore zeolite (ring opening 3.6 Å) with a chabazite framework; its structure contains a 3D pore system limited by 8-member rings. The main characteristics of these zeolitic frameworks are reported in Table 1, together with the compositional and textural characterization.

As expected, all the zeolites are characterized by a large surface area and very low pore volume; the addition of Pd does not substantially modify either the surface area or the pore volume.

X-ray Diffraction (XRD) patterns obtained on the bare zeolites and on the Pd-doped samples (Figure 1) are in agreement with the diffraction patterns for the reference zeolite frameworks [22]. The zeolite structure is maintained in all the catalysts even after Pd addition; additionally, peaks corresponding to crystalline PdO, whose most intense peak should be observed at 33.8° (JCPDS 75-0584), are not observed, suggesting that particles are too small to be identified by the XRD technique or absent.

SEM (Scanning Electron Microscopy) images reported in Figure 2 clearly show the maintenance of the zeolite morphologies also after Pd addition; moreover, the associated energy-dispersive X-ray (EDX) analysis confirms the Si/Al ratio given by the supplier and

the Pd loading near the nominal value (1 wt%, see Table 1). Pd loading has also been confirmed by ICP-MS analysis in the case of the SSZ-13 sample.

Table 1. Morphological and chemico-physical characteristics of bare zeolites and Pd-doped ones.

Sample	Framework Structures and Pore System	Pore Sizes (Å)	Si/Al Ratio ^a	Pd Loading (%) ^a	BET (m ² /g)	V _p (cm ³ /g)
Y	FAU; 3D;	7.4	30	//	616	0.27
Pd/Y	12-ring channels			1.07	612	0.27
ZSM-5	MFI; 2D;	5.4–5.6	40	//	407	0.10
Pd/ZSM-5	10-ring channels			1.07	390	0.12
FER	FER; 2D;	4.3–5.5	11	//	302	0.13
Pd/FER	10 and 8-ring channels			1.1	312	0.10
SSZ-13	CHA; 3D;	3.6–3.7	10	//	558	0.09
Pd/SSZ-13	8-ring channels			1.14 ^b	578	0.06

^a from EDX analysis. ^b 1.03% from ICP-MS analysis.

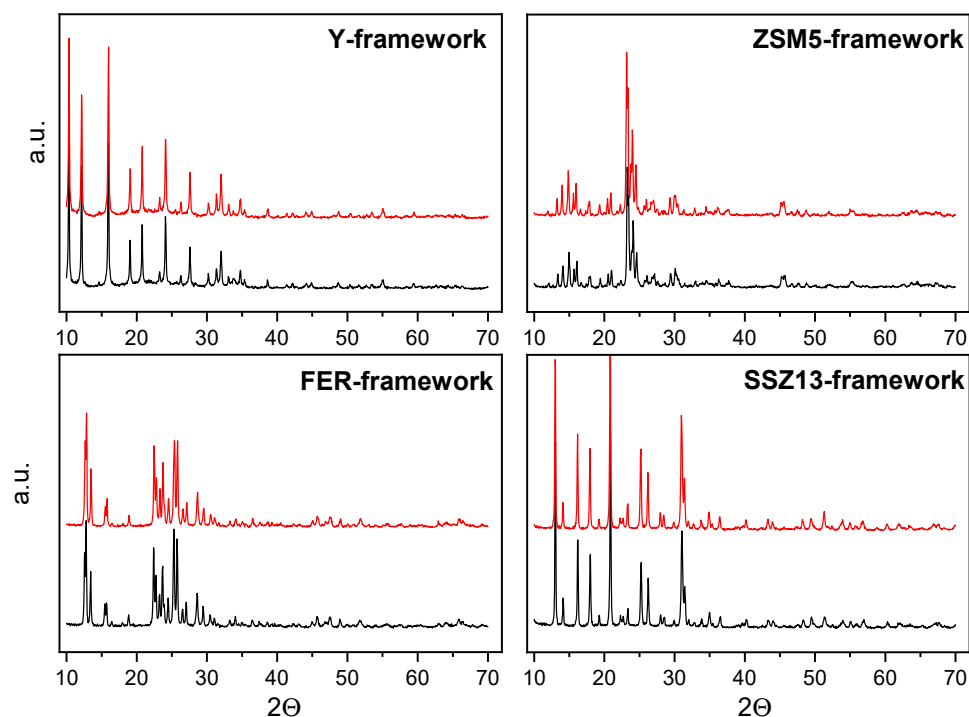


Figure 1. X-ray diffraction (XRD) patterns of zeolite (red line) and Pd/zeolite on different frameworks (black line).

2.1.2. FT-IR Characterization

CO adsorption—In Figure 3, the FT-IR spectra of CO (20 mbar) adsorbed at Room Temperature (RT) on the activated samples are displayed. The spectra are characterized by complex envelopes of bands, which are related to Pd carbonyl species in different oxidation states and coordination, as discussed in our previous paper [23], where the precise assignment of each component in the spectrum of Pd/SSZ-13 was made. As discussed in ref. [23], with reference to the Pd/SSZ-13 sample (trace a), it is possible to divide the bands into different spectral regions, namely 2220–2170 cm⁻¹ and 2170–2110 cm⁻¹, associated with linear carbonyls of Pd²⁺ and Pd⁺, respectively [13,24–26]. The absorption near 2228 cm⁻¹ is assigned to carbonyls of extra-framework Al³⁺ [27].

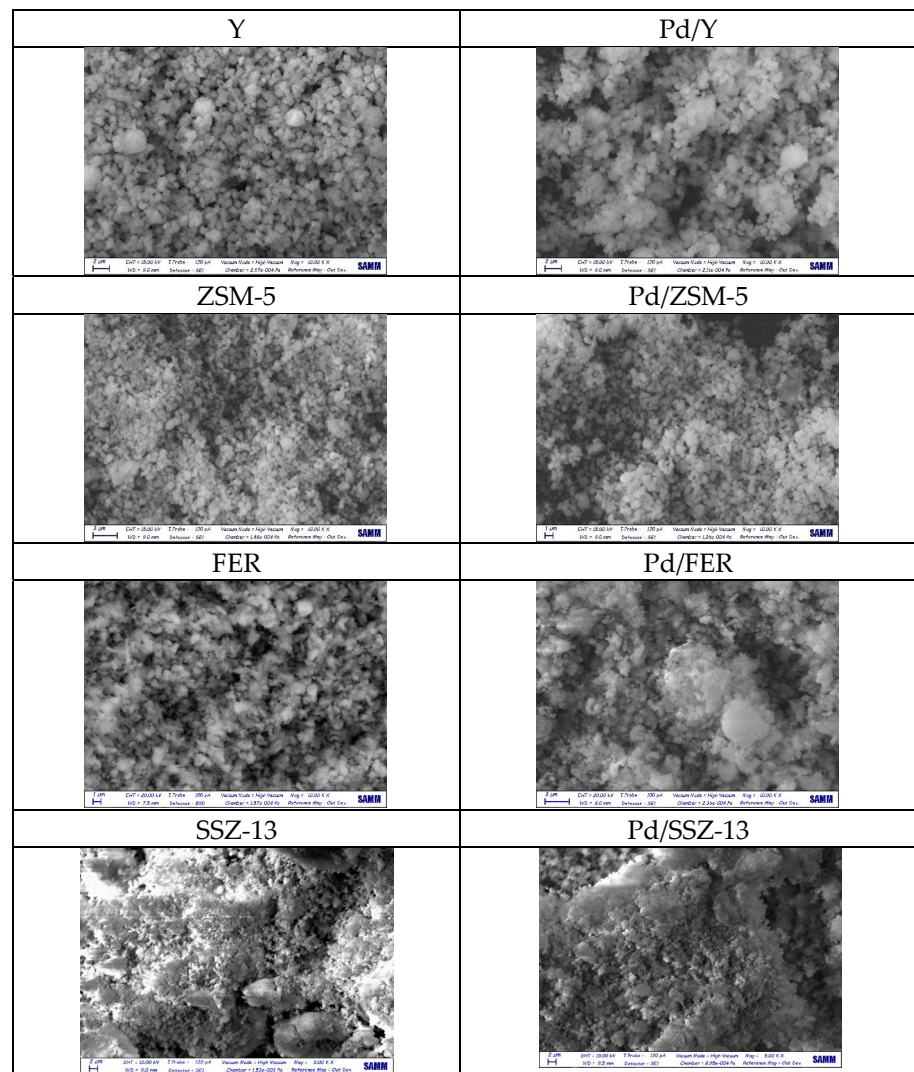


Figure 2. SEM images of bare zeolites and of the corresponding Pd-doped samples.

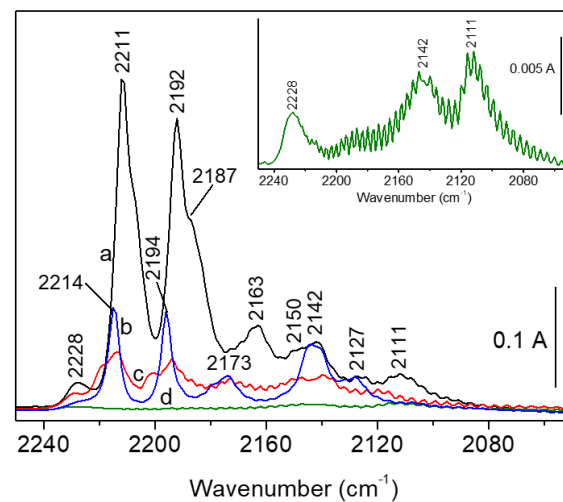


Figure 3. FT-IR spectra of CO (20 mbar) adsorbed at RT on activated Pd/SSZ-13 (a—black line), Pd/ZSM-5 (b—blue line), Pd/FER (c—red line), and Pd/Y (d—green line).

In the spectral region 2220–2170 cm^{-1} (where very strong bands are present in the case of Pd/SSZ-13 sample, Figure 3 trace a), it has to be considered that, due to the σ -donation contribution in the Pd^{2+} -CO bond, the higher the band frequency, the more coordinatively unsaturated the site. With this in mind and on the base of the literature data, the bands at 2211 and 2192 cm^{-1} are assigned to di-carbonyls ($\nu_{\text{asym}}(\text{CO})$ and $\nu_{\text{sym}}(\text{CO})$ modes, respectively) of isolated Pd^{2+} ions formed by ion exchange with the Brønsted acid sites of the zeolite [24,28]; the shoulder at 2187 cm^{-1} is instead assigned to CO adsorbed on Pd^{2+} sites of PdO_x particles [23].

Along similar lines, for the spectral region 2170–2110 cm^{-1} , due to the π -backdonation contribution to the Pd^+ -CO bond, the lower the band frequency, the more coordinatively unsaturated the site. For this reason, in the spectrum of Pd/SSZ-13 (Figure 3, trace a), the band at 2163 cm^{-1} is assigned to CO adsorbed on Pd^+ sites belonging to PdO_x particles. The bands at 2150, 2142, 2127, and 2111 cm^{-1} are related to the presence of two different Pd^+ di-carbonyl species (two couple of bands, one component of the couple related to $\nu_{\text{asym}}(\text{CO})$ mode, the other component to $\nu_{\text{sym}}(\text{CO})$ mode), whose presence is well demonstrated in our previous paper [23]. This implies, for Pd/SSZ-13, the existence of two different isolated Pd^+ sites formed by ion exchange with the Brønsted acid sites of the zeolite: indeed, Pd^+ can be located into both 8- and 6-member rings of the zeolite framework [17,29].

For Pd/ZSM-5 and Pd/FER samples (Figure 3, traces b and c, respectively), the bands observed in the same regions are less intense, but their assignments are similar to that examined for the Pd/SSZ-13 sample. In particular, for the Pd/ZSM-5 sample, the bands at 2214 and 2194 cm^{-1} are assigned to di-carbonyls of isolated Pd^{2+} ions; the band at 2173 cm^{-1} to CO bonded on Pd^{2+} belonging to PdO particles; the bands at 2142 and 2127 cm^{-1} to di-carbonyls of isolated Pd^+ sites. For the Pd/FER sample (Figure 3, trace c), the broadness of the bands means higher surface heterogeneity. Notably, the two bands related to di-carbonyls of isolated Pd^{2+} ions at about 2214 and 2194 cm^{-1} show shoulders, pointing out the presence of exchanged Pd^{2+} ions located in different zeolite positions (e.g., 10- and 8-ring channels). Finally, it is worth noting that the spectrum of Pd/Y (Figure 3, trace d) shows very weak bands, enlarged in the inset of Figure 3. Only bands related to di-carbonyls of isolated Pd^+ ions are present at 2142 and 2111 cm^{-1} , respectively. The band at 2228 cm^{-1} related to carbonyls of extra-framework Al^{3+} is present as well.

The area of the carbonyl bands is proportional to the number of available Pd sites, both isolated Pd species inside the zeolite framework and Pd species belonging to external PdO_x particles. Inspection of Figure 3 clearly indicates that the availability of the Pd sites (i.e., the dispersion) is highest for the Pd/SSZ-13 sample and follows the order: Pd/SSZ-13 > Pd/ZSM-5 ~ Pd/FER >> Pd/Y. This suggests a relationship between pore size and the Pd dispersion: the smaller the pore size, the higher the Pd dispersion. In this respect, it has to be recalled that Zheng et al. [13] characterized Pd on zeolites with different pore sizes and found that Pd is largely present as isolated ions in the ZSM-5 framework, while the small pore opening of SSZ-13 inhibits the exchange with Brønsted acid sites. In our case, the availability of the Pd sites follows a different order, as reported above, apparently in contrast with the results of Zheng et al. This discrepancy might be related to the different pretreatment of the samples: in fact, while they evaluated the dispersion of isolated Pd ions on the freshly calcined samples, at variance, we evaluated the dispersion after an activation treatment in vacuum and oxygen at 500 °C.

In addition, our results seem to indicate that the Pd dispersion is not driven by the Si/Al ratio for zeolites having similar pore size: in fact, the Pd/ZSM-5 and Pd/FER samples, characterized by similar pore size but different Si/Al ratio, exhibit similar Pd dispersion. This suggests that the Pd dispersion, for the Pd loading conditions here adopted, is primarily affected by the zeolite pore size and only to a minor extent by the Si/Al ratio. At variance, Khivantsev et al. [28] analyzed the Pd dispersion over 1 wt% Pd-doped zeolites having different Si/Al ratios (and the same framework) but prepared in a different way and observed that the Si/Al ratio significantly affects the Pd dispersion. In particular, these authors, using a modified-ion exchange method to prepare 1 wt% Pd on NH_4 -SSZ-13 with

Si/Al ratios ranging from 6 to 30, observed the increasing formation of PdO nanoparticles (i.e., low dispersion) upon increasing the Si/Al ratio. This is very likely related to the different preparation method used by these authors, which significantly differs with respect to our preparation route.

NO and NO/O₂ adsorption—Traces “a” in Figure 4 show FT-IR spectra of NO adsorbed at RT on activated Pd/Y (A), Pd/ZSM-5 (B), Pd/FER (C), and Pd/SSZ-13 (D). In all cases, bands in the region of 1900–1800 cm⁻¹ are present with intensities that vary from one sample to another. These spectral features are well documented in the literature and are assigned to nitrosyl species of Pd²⁺ and Pd⁺, even if there is no definitive consensus on the precise assignments of the single bands to either the Pd²⁺ or Pd⁺ species [28–32]. Accordingly, it is worth noting that, contrarily to CO, NO adsorption is not able to distinguish the different coordinations of Pdⁿ⁺ ions (isolated ions or sites on particles). In fact, the complex envelopes of bands present in the spectra of adsorbed CO do not find correspondence in the spectral features shown upon NO adsorption. However, the intensities of the Pd nitrosyl bands in the various samples well match those of carbonyls observed upon CO adsorption. This confirms the Pd dispersion order already discussed in the case of CO adsorption, i.e., Pd/SSZ-13 > Pd/ZSM-5 ~ Pd/FER >> Pd/Y.

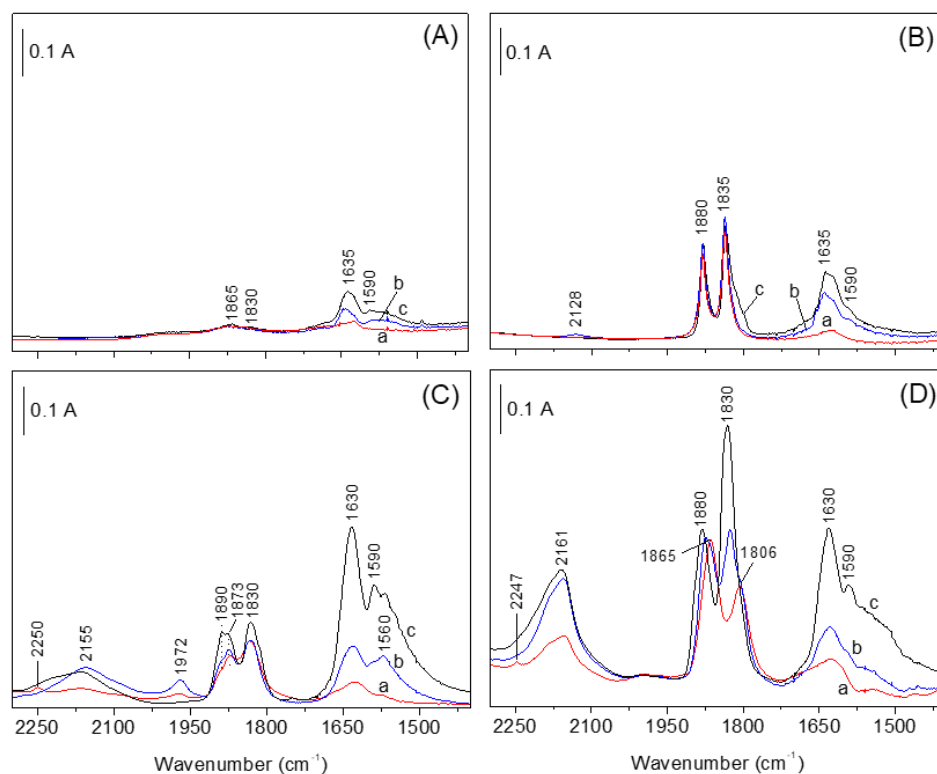
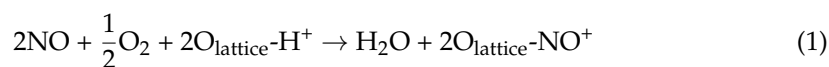


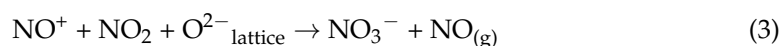
Figure 4. FT-IR spectra of NO (2 mbar, curves a—red) adsorbed at RT on activated Pd/Y (A), Pd/ZSM-5 (B), Pd/FER (C), and Pd/SSZ-13 (D). Curves b (blue) and c (black): NO/O₂ mixture (1:5, p_{NO} = 2 mbar) after 5 and 60 min of contact at RT, respectively.

Along with Pd nitrosyl bands, for Pd/FER and Pd/SSZ-13 samples (Figure 4, traces “a”, sections C and D, respectively), peaks at 2250–2247, 2161–2155, 1972 (only for Pd/FER), and at about 1630 cm⁻¹ are also present. The bands at 2250–2247 cm⁻¹ and at 1972 cm⁻¹ are related to adsorbed N₂O and N₂O₃, respectively, present as impurities in the gas [33] or formed as detailed below. On the other hand, the bands at 2161–2155 and 1630 cm⁻¹ are assigned to the stretching mode of NO⁺ and to the bending mode of adsorbed molecular

water, respectively. Hadjiivanov et al. [34] proposed the formation of these species upon the reaction of NO with Brønsted acid sites of an H-ZSM-5 in the presence of oxygen:



Oxygen is not present in the gas phase, but the samples were oxidized before NO admission: accordingly, oxygen species are likely present on the Pd phase. This is supported by the fact that the bands related to NO^+ and adsorbed molecular water show lower intensities on the sample with lower Pd dispersion, i.e., Pd/FER with respect to Pd/SSZ-13. As a matter of fact, NO^+ species are observable with very low intensities also in the Pd/ZSM-5 sample (NO^+ band at 2128 cm^{-1} and water band at 1635 cm^{-1}), and they are not present (except for a very small amount of water) for Pd/Y sample, for which Pd site availability is almost nil. It is important to point out that the presence of reactive oxygen species on the Pd phase can also induce the formation of NO_2 that, along with NO, can form the adduct N_2O_3 (indeed observed for Pd/FER catalyst) and/or can form NO^+ and surface nitrates according to the following reactions [35–37]:



Consequently, the observed NO^+ can be derived from both reactions (1) and (2), along with nitrates that should show characteristic vibrational modes in the region below 1700 cm^{-1} . As a matter of fact, nitrates could contribute to the band at about 1630 cm^{-1} , assigned to the bending mode of molecular water. All these observations were confirmed by oxygen admission, as described in the following section.

Starting from the condition obtained in the presence of 2 mbar of NO (spectra “a”), 10 mbar of oxygen were added: traces “b” and “c” in the different sections of Figure 4 show the evolution of bands after 5 and 60 min, respectively. First of all, the increase in bands below 1700 cm^{-1} , assigned to surface nitrates formed by reactions (2) and (3) mentioned above, where NO_2 is formed upon NO oxidation, is well evident for all the samples. In this region, the band at 1630 cm^{-1} is related to both nitrates and molecular water formed by reaction (1). Moreover, reactions (1) and (2) account for the formation of NO^+ , whose band suddenly increases after oxygen admission for Pd/SSZ-13 and Pd/FER samples. Even in the presence of oxygen, the band of NO^+ at 2128 cm^{-1} remains very weak for Pd/ZSM-5 and not detectable for Pd/Y sample. Indeed, reaction (1) needs Brønsted acid sites to occur: as a matter of fact, the intensity of the band and hence the amount of adsorbed NO^+ is directly related to the Brønsted acid site amount, i.e., to the Si/Al ratio of the zeolite. Moreover, it has to be taken into account the higher stability of adsorbed NO^+ in the smaller channels of SSZ-13 and FER [38].

Concerning nitrosyl species, oxygen admission causes an intensity increase in the bands for Pd/SSZ-13 and Pd/FER samples. Moreover, for Pd/SSZ-13 sample, nitrosyl bands blue-shift upon oxygen admission. The latter can be ascribed to the increase in the average positive charge of the Pd sites, especially of the Pd^+ sites, induced by oxygen adsorption, which could also cause changes in the absorption coefficients of nitrosyl species, justifying the increase in band intensities.

The areas (integrated intensities) of the bands related to nitrosyls and nitrates are indicative of the Pd dispersion, as also evidenced by CO adsorption. Indeed, along with nitrosyl formation, the presence of Pd is required to form nitrate species as well. In fact, nitrates are not formed in the absence of Pd, as evidenced by the comparison between the NO/O_2 adsorption on Pd/SSZ-13 and the bare SSZ-13 shown in Figure 5. This comparison also points out the markedly lower amount of NO^+ (band at 2161 cm^{-1}) on Pd/SSZ-13 with respect to the bare zeolite. In fact, NO^+ is formed on the zeolite Brønsted acid sites,

and their concentration has been reduced as a result of Pd exchange with the formation of Pd²⁺ and Pd⁺ sites.

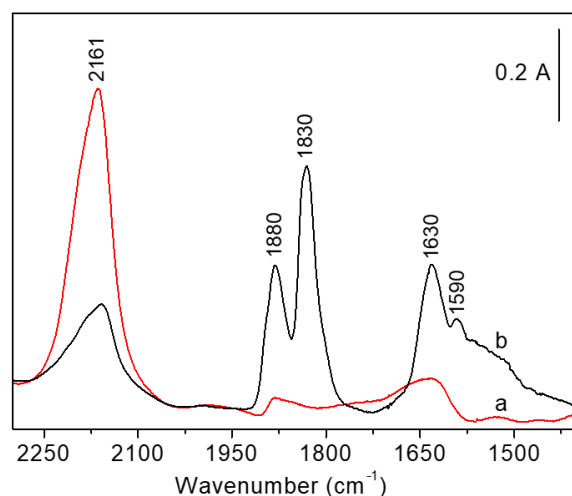


Figure 5. FT-IR spectra of NO/O₂ mixture (1:5, p_{NO} = 2 mbar) adsorbed at RT after 60 min of contact on activated SSZ-13 (a) and Pd/SSZ-13 (b).

2.2. NO_x Uptake and Desorption Experiments

2.2.1. NO/O₂ Adsorption Phase

The NO_x storage performances of Pd/zeolite were determined under realistic conditions, i.e., at 80 °C with a NO/O₂ mixture in the presence of CO₂ and H₂O.

The concentration traces obtained upon NO_x adsorption and subsequent Temperature Programmed Desorption (TPD) are shown in Figure 6A–D. For all samples, upon the addition of the NO/O₂ mixture, the NO concentration recorded at the reactor outlet rapidly increases without showing any dead time, eventually reaching the inlet concentration value with a dynamic response that depends on the catalyst sample. The response is very fast in the case of Pd/Y (Figure 6A) and sluggish for the Pd/SSZ-13 sample (Figure 6D), which, in fact, shows a large NO_x uptake evaluated from the amounts of desorbed NO_x during the TPD (Figure 7). Lower amounts of NO_x are stored on the other Pd-doped samples, and the following order is observed: Pd/SSZ-13 > Pd/ZSM-5 ~ Pd/FER >> Pd/Y (Figure 7). This ranking is in good agreement with the Pd dispersion evaluated from FT-IR measurements of CO and NO adsorption.

During NO adsorption, NO₂ evolution is also observed, although with different features. In fact, a small NO₂ peak is observed in the case of Pd/ZSM-5 and Pd/FER (Figure 6B, C, respectively), with evolution of 8 and 5 μmol/g_{cat} NO₂, respectively, whereas a sluggish NO₂ evolution is seen in the case of Pd/SSZ-13. The overall amount of NO₂ evolved, in this case, is near 19 μmol/g_{cat}. Almost no NO₂ formation is observed in the case of Pd/Y.

NO₂ evolution observed during the adsorption phase is likely related to the reduction of Pd²⁺ to Pd⁺ operated by NO according to the following overall reaction [13,39–41]:



According to the stoichiometry of reaction (4), 3 moles of NO are consumed and lead to the formation of 1 mol of NO₂ evolved in the gas phase and to the storage of 2 moles of Pd nitrosyls. Reaction (4) also envisages the reduction of Pd²⁺ with the formation of Pd⁺ nitrosyls upon NO adsorption.

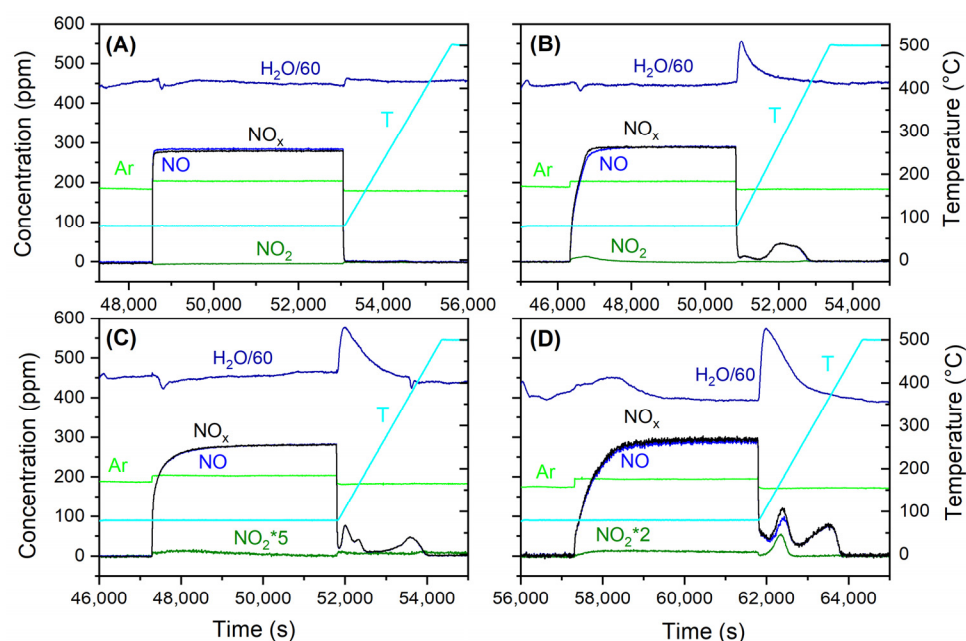


Figure 6. NO/O₂ adsorption at 80 °C and subsequent TPD experiment over the activated zeolite-based samples: (A) Pd/Y; (B) Pd/ZSM-5; (C) Pd/FER; and (D) Pd/SSZ-13. Experimental conditions: storage phase NO (300 ppm) + O₂ (3%) + CO₂ (2%) + H₂O (2.5%) in He; TPD in O₂ (3%) + CO₂ (2%) + H₂O (2.5%) in He from 80 °C to 500 °C (10°/min). Note that NO₂ traces have been multiplied by 5 (panel C) or 2 (panel D).

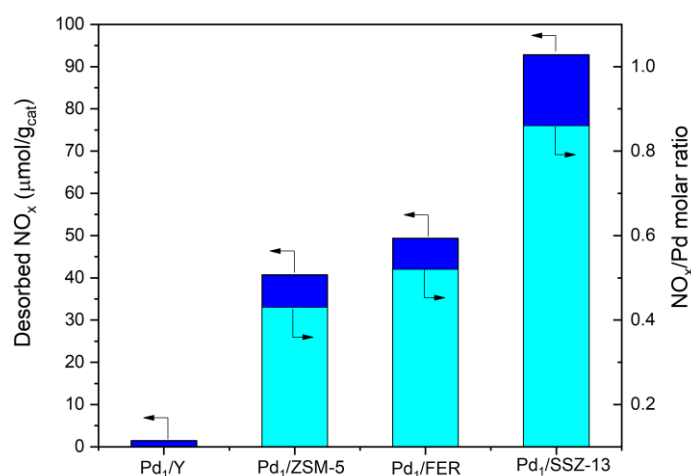


Figure 7. Quantitative analysis of NO_x desorbed (dark blue) and NO_x/Pd ratio (light blue) after adsorption of NO/O₂ at 80 °C.

Notably, as expected from the stoichiometry of reaction (4), the amounts of evolved NO₂ represent half of the amounts of formed nitrosyls. However, as will be shown in the following section, the amounts of stored NO_x are higher than those expected from the stoichiometry of reaction (4) based on the NO₂ formation. This points out that other routes are active in the storage of NO_x, possibly involving the direct NO uptake on Pd²⁺ sites as well.

2.2.2. NO_x Desorption Phase

During the thermal desorption (TPD) after the NO/O₂ storage at 80 °C, NO_x release occurs mainly as NO, although NO₂ is also observed to desorb. The amounts of evolved NO_x were evaluated from the area of the TPD peaks, and the results are summarized in Figure 7, along with the estimated desorbed NO_x/Pd molar ratio.

For all samples, at the beginning of the temperature ramp a desorption of H₂O is observed due to the heating ramp; notably, the amounts of water desorbed is inversely proportional to the pores size, i.e., the bigger the pores, the lower the amount of desorbed water. This is very likely related to water capillary condensation that is favored within the smaller pores.

In the case of the Pd/SSZ-13 sample (Figure 6D), three main desorption regions can be identified: (i) from the closure of the NO/O₂ feed up to 120 °C a tail is apparent due to the physisorbed species, counting for 13 μmol/g_{cat} NO; (ii) from 120 °C to 240 °C a well-defined peak is observed with a maximum at 180 °C, composed of NO and NO₂ (32 μmol/g_{cat} and 6 μmol/g_{cat}, respectively); and (iii) a high temperature peak (in the range of 240–500 °C) formed only by NO (41.4 μmol/g_{cat}) and centered near 360 °C. The overall amount of evolved NO_x is near 93 μmol/g_{cat} (see Figure 7). As previously recalled, the overall amounts of stored NO_x are well above those expected from the amounts of evolved NO₂, based on the stoichiometry of reaction (4). This indicates the occurrence of other adsorption reactions besides reaction (4), e.g., direct NO uptake on Pd²⁺ with no reduction of Pd²⁺ to Pd⁺ (and no NO₂ formation).

The Pd/ZSM-5 and Pd/FER present two desorption regions (Figure 6B,C, respectively), the former in the low-temperature region below 240 °C and the latter in the high-temperature region above 300 °C; negligible amounts of NO₂ are observed for these samples. The overall amounts of desorbed NO_x are 41 and 50 μmol/g_{cat}, respectively. Finally, in the case of Pd/Y (Figure 6A), any NO_x desorption is observed, as expected, due to the negligible storage capacity of this sample. These results are well in line with the CO and NO FTIR adsorption experiments previously discussed, showing a higher NO adsorption capacity for Pd/SSZ-13.

From the amounts of stored NO_x, we have also estimated the adsorbed NO_x/Pd molar ratio (Figure 7) under the hypothesis that all NO_x are stored over Pd. In the case of the Pd/SSZ-13 sample, a value of desorbed NO_x near 93 μmol/g_{cat} was evaluated, corresponding to a NO_x/Pd molar ratio of 0.86. This calls for a large utilization of Pd, thus indicating a good dispersion of the metal. The Pd/ZSM-5 and Pd/FER showed lower stored NO_x/Pd values, whereas, as already stated the storage capacity for Pd/Y is negligible.

Concerning the stability of the adsorbed NO_x species, low- and high-temperature contributions are observed in all cases, excluding the Pd/Y sample that shows no NO adsorption. NO_x desorption peaks at low and high temperatures (near 150 °C and 360 °C) have also been observed, e.g., by Gupta et al. over Pd/SSZ-13 [39]; the authors attributed these two peaks to at least two different adsorption sites with distinct binding energies. In particular, they attributed the lower temperature NO peak to NO bound to Z⁻Pd²⁺Z⁻ (where Z⁻ denotes the zeolite anionic aluminum site (Al-O-Si)⁻) and the higher temperature NO peak to NO bound to Z⁻Pd⁺. Similar conclusions have been drawn by Villamaina et al. [37], who pointed out that more stable nitrosyls are formed over Pd⁺ species. Moreover, as reported by Castoldi et al. in the case of Pd/FER [42], and by Matarrese et al. [23] for Pd/SSZ-13, the low-temperature NO_x desorption peak can also be associated with the decomposition of nitrate species. On this basis, it is speculated that the low-T desorption peaks can be associated with the decomposition of nitrates and/or Pd²⁺ nitrosyls, whereas the high desorption peak is related to the decomposition of stable Pd⁺ nitrosyls.

The results reported above clearly indicate that the zeolite framework affects both the amounts and the stability of the stored NO_x. The characterization data previously discussed point out the existence of different Pd species in terms of different structures and oxidation states, including isolated Pd cations and PdO_x particles on the external zeolite surface, whose distribution varies with the zeolite framework [11,13]. Additionally, according to FT-IR characterization, the investigated samples show different Pd dispersion, and evidence has been provided on the fact that this parameter is influenced by the pore size of the zeolitic framework. The Pd dispersion is the key parameter affecting the NO_x storage, having observed a clear correlation between NO_x adsorption capacity and Pd dispersion.

Notably, a very high NO adsorption capacity has been measured for the Pd/SSZ-13 sample, in spite of the fact that Pd species belonging to PdO_x particles have been identified by CO adsorption. This suggests that also non-isolated Pd species participate in the NO_x storage.

3. Materials and Methods

3.1. Sample Preparation

The Pd-doped zeolites (Pd/Y, Pd/ZSM-5, Pd/FER, and Pd/SSZ-13; Pd loading 1% w/w) used in this study were prepared starting from commercial samples (Zeolyst International, Kansas City, KS, USA and ACS Material LLC, Pasadena, CA 91106) in their NH₄- or H-form. The zeolites in the NH₄-form were transformed into H-form by calcination at 700 °C in the air (heating rate: 1 °C/min).

Then, the Pd-doped zeolite samples were prepared by impregnation of the zeolite supports in excess of solvent using aqueous Pd(NO₃)₂ (solution at 4.5% Pd, Sigma-Aldrich, St. Louis, MO, USA), followed by drying in air at 80 °C overnight [42]. The dried precursors were calcined from room temperature up to 500 °C (rate: 1 °C/min, at 500 °C 3 h) and then from 500 °C up to 750 °C (rate 5 °C/min, at 750 °C 2 h).

3.2. Sample Characterization

BET analysis was performed by adsorption–desorption of nitrogen at −196 °C using a Micromeritics Tristar 300 instrument (Alfatest SRL, Rome, Italy). Before the measurement, samples were outgassed at 120 °C and 0.1 torr for 3 h.

Powder X-ray diffraction (XRD) patterns of bare and Pd/zeolite samples were obtained using a Bruker D8 diffractometer () with Cu K α radiation. The XRD patterns were obtained on the as prepared samples in the range of 10–50° (2 θ) with a step size of 0.05° at a speed of 12.5°/min.

SEM and elemental compositions analysis of bare zeolite and Pd-doped samples were performed using a ZEISS EVO 50 instrument (Oberkochen, Germany) equipped with energy-dispersive X-ray analyzer (EDX) model Quantax 200 6/30 (Bruker, Karlsruhe, Germany).

ICP-MS analysis has been performed on selected samples to evaluate the Pd loading. The Perkin Elmer NexION 2000 single quadrupole ICP-MS instrument (Shelton, CT, USA) was employed upon calibration with a limit of quantification (LOQ) of 0.040 ppb for Pd.

IR spectra were run in transmission mode at RT on a Perkin-Elmer FT-IR 2000 spectrophotometer (Shelton, CT, USA) equipped with a Hg-Cd-Te cryodetector, working in the range of wavenumbers 7200–580 cm^{−1} at a resolution of 2 cm^{−1} (number of scans ~60). Self-supporting disks (10–15 mg cm^{−2}) were obtained from the powder samples and placed in a quartz IR cell allowing thermal treatments in vacuum or in a controlled atmosphere. The samples were activated by treatment at 500 °C in vacuum, followed by oxidation in dry O₂ (40 mbar) at the same temperature. The samples were cooled down to room temperature (RT) in oxygen. CO adsorption was performed to characterize the nature and availability of Pd sites; NO and NO/O₂ adsorptions were performed to evidence the species formed during NO_x storage. IR spectra were recorded at RT in static conditions before and after interaction with CO (20 mbar), NO (2 mbar), and NO/O₂ (1:5, p_{NO} = 2 mbar) mixture. In the figures, spectra are reported as difference spectra, where the subtrahend spectrum is that of the sample after the activation, before the admission of the gas.

3.3. Gas phase Analysis during NO/O₂ Adsorption at Low Temperature

NO_x adsorption experiments were conducted using 100 mg of powdered samples, sieved at 70–100 μ m, and loaded in a quartz microreactor with an internal diameter of 8 mm. The outlet of the reactor is directly connected to a mass spectrometer (ThermoStar 200, Pfeiffer Vacuum GmbH, Aßlar, Germany), a UV-analyzer specific for NO, NO₂, NH₃ (Limas 11 HW, ABB, Zurig, Switzerland), and a micro gas-chromatograph (3000 A, Agilent, Santa Clara, CA 95051 United States). In a typical experiment, the sample was initially pre-treated at 500 °C for 30 min under a flow of O₂ (3% v/v), CO₂ (2% v/v), and H₂O (2.5% v/v) (balance He) at a flow rate of 100 Ncm³/min. The sample was then cooled

down to the adsorption temperature (50 °C, 80 °C, or 120 °C) without changing the gas flow composition, and at this temperature 300 ppm of NO were stepwise added to the gas mixture for 75 min. Then, the NO supply was closed, and the sample was heated under temperature programming (TPD) up to 500 °C (heating rate 10 °C/min).

4. Conclusions

In this study, Pd-promoted zeolites have been prepared by impregnation of the zeolite supports in excess of solvent and investigated for potential use in low-temperature NO_x adsorption. Four zeolitic supports with different structures have been considered (Y, ZSM-5, FER, and SSZ-13). These structures have different pore openings, i.e., large (Y), medium (ZSM-5 and FER), and small (SSZ-13); samples with different Si/Al ratios have also been considered. All the samples have been characterized and tested in the adsorption of NO under relevant operating conditions.

The FT-IR characterization using CO as a probe molecule evidenced the presence of a variety of Pdⁿ⁺ sites with different coordination. In particular, isolated Pd cations formed by ion exchange with the Brønsted acid sites of the zeolite and on the surface of PdO_x particles have been evidenced. The Pd dispersion estimated by CO and NO adsorption follows the order: Pd/SSZ-13 > Pd/ZSM-5 ~ Pd/FER >> Pd/Y, i.e., increases upon decreasing the pore opening. These results suggest that the pore size plays a primary role in controlling the Pd dispersion. At variance, the relevance of the Si/Al ratio in affecting the Pd dispersion seems to be minor. In other words, the zeolite structure (and related pore openings) is apparently the key parameter to drive the Pd dispersion.

Reactivity experiments carried out under the relevant conditions pointed out that the amounts of adsorbed NO_x follow the same order as the Pd dispersion. Notably, a very high NO_x/Pd molar ratio has been estimated for Pd/SSZ-13, despite the presence of PdO_x clusters and/or particles pointed out in this sample besides well-dispersed Pd sites. This suggests that non-isolated Pd species belonging to particles participate in the NO_x storage along with isolated well-dispersed species.

Author Contributions: P.T.: Investigation, Methodology. L.C.: Investigation, Conceptualization, Writing—original, review & editing, Methodology. S.M.: Investigation, Writing—original, review & editing, Conceptualization, Funding acquisition. R.M.: Writing—review & editing, Conceptualization. L.L.: Supervision, Conceptualization, Writing—review & editing. All authors have read and agreed to the published version of the manuscript.

Funding: This research received no external funding.

Data Availability Statement: The data presented in this study are available in Catalysts 2023, 13.

Acknowledgments: S.M. and P.T. acknowledge the support from Project CH4.0 under the MUR (Italian Ministry for the University) program “Dipartimenti di Eccellenza 2023–2027” (CUP: D13C22003520001).

Conflicts of Interest: The authors declare no conflict of interest.

References

1. Körfer, T. *Potential of Advanced, Combined Aftertreatment Systems for Light-Duty Diesel Engines to Meet Upcoming EU and US Emission Regulation*; SAE Technical Paper 2013-24-0163; SAE International: Warrendale, PA, USA, 2013.
2. Roy, S.; Baiker, A. NO_x Storage-Reduction Catalysis: From Mechanism and Materials Properties to Storage-Reduction Performance. *Chem. Rev.* **2009**, *109*, 4054–4091. [[CrossRef](#)]
3. Epling, W.S.; Campbell, L.E.; Yezerets, A.; Currier, N.W.; II, J.E.P. Overview of the Fundamental Reactions and Degradation Mechanisms of NO_x Storage/Reduction Catalysts. *Catal. Rev.* **2004**, *46*, 163–245. [[CrossRef](#)]
4. Olsson, L.; Wijayanti, K.; Leistner, K.; Kumar, A.; Joshi, S.Y.; Kamasamudram, K.; Currier, N.W.; Yezerets, A. A kinetic model for sulfur poisoning and regeneration of Cu/SSZ-13 used for NH₃-SCR. *Appl. Catal. B Environ.* **2016**, *183*, 394–406. [[CrossRef](#)]
5. Theis, J.R.; Lambert, C.K. An assessment of low temperature NO_x adsorbers for cold-start NO_x control on diesel engines. *Catal. Today* **2015**, *258*, 367–377. [[CrossRef](#)]
6. Gao, Z.; Kim, M.-Y.; Choi, J.-S.; Daw, C.S.; Parks, J.E.; Smith, D.E. Cold-start emissions control in hybrid vehicles equipped with a passive adsorber for hydrocarbons and nitrogen oxides. *Proc. Inst. Mech. Eng. Part D J. Automob. Eng.* **2012**, *226*, 1396–1407. [[CrossRef](#)]

7. Tamm, S.; Andonova, S.; Olsson, L. Silver as Storage Compound for NO_x at Low Temperatures. *Catal. Lett.* **2014**, *144*, 674–684. [[CrossRef](#)]
8. Jones, S.; Ji, Y.; Crocker, M. Ceria-Based Catalysts for Low Temperature NO_x Storage and Release. *Catal. Lett.* **2016**, *146*, 909–917. [[CrossRef](#)]
9. Gu, Y.; Epling, W.S. Passive NO_x adsorber: An overview of catalyst performance and reaction chemistry. *Appl. Catal. A Gen.* **2019**, *570*, 1–14. [[CrossRef](#)]
10. Lee, J.; Theis, J.R.; Kyriakidou, E.A. Vehicle emissions trapping materials: Successes, challenges, and the path forward. *Appl. Catal. B Environ.* **2019**, *243*, 397–414. [[CrossRef](#)]
11. Chen, H.-Y.; Collier, J.E.; Liu, D.; Mantarosie, L.; Durán-Martín, D.; Novák, V.; Rajaram, R.R.; Thompsett, D. Low Temperature NO Storage of Zeolite Supported Pd for Low Temperature Diesel Engine Emission Control. *Catal. Lett.* **2016**, *146*, 1706–1711. [[CrossRef](#)]
12. Murata, U.; Morita, T.; Wada, K.; Ohno, H. NO_x Trap Three-Way Catalyst (N-TWC) Concept: TWC with NO_x Adsorption Properties at Low Temperatures for Cold-Start Emission Control. *SAE Int. J. Fuels Lubr.* **2015**, *8*, 454–459. [[CrossRef](#)]
13. Zheng, Y.; Kovarik, L.; Engelhard, M.H.; Wang, Y.L.; Wang, Y.; Gao, F.; Szanyi, J. Low-Temperature Pd/Zeolite Passive NO_x Adsorbers: Structure, Performance, and Adsorption Chemistry. *J. Phys. Chem. C* **2017**, *121*, 15793–15803. [[CrossRef](#)]
14. Ryou, Y.; Lee, J.; Lee, H.; Kim, C.H.; Kim, D.H. Low temperature NO adsorption over hydrothermally aged Pd/CeO₂ for cold start application. *Catal. Today* **2018**, *307*, 93–101. [[CrossRef](#)]
15. Lee, J.; Ryou, Y.; Cho, S.J.; Lee, H.; Kim, C.H.; Kim, D.H. Investigation of the active sites and optimum Pd/Al of Pd/ZSM-5 passive NO adsorbers for the cold-start application: Evidence of isolated-Pd species obtained after a high-temperature thermal treatment. *Appl. Catal. B Environ.* **2018**, *226*, 71–82. [[CrossRef](#)]
16. Lee, J.; Ryou, Y.; Hwang, S.; Kim, Y.; Cho, S.J.; Lee, H.; Kim, C.H.; Kim, D.H. Comparative study of the mobility of Pd species in SSZ-13 and ZSM-5, and its implication for their activity as passive NO_x adsorbers (PNAs) after hydro-thermal aging. *Catal. Sci. Technol.* **2019**, *9*, 163–173. [[CrossRef](#)]
17. Pace, R.B.; Lardinois, T.M.; Ji, Y.; Gounder, R.; Heintz, O.; Crocker, M. Effects of Treatment Conditions on Pd Speciation in CHA and Beta Zeolites for Passive NO_x Adsorption. *ACS Omega* **2021**, *6*, 29471–29482. [[CrossRef](#)]
18. Wang, Y.; Shi, X.; Liu, Z.; Shan, Y.; Shi, W.; Yu, Y.; He, H. The study of Pd-SSZ-13 as low-temperature passive NO adsorber materials: High dispersal of Pd in small-pore CHA zeolites by thermal treatment. *Appl. Catal. B Environ.* **2023**, *324*, 122254. [[CrossRef](#)]
19. Theis, J.R.; Ura, J.; Getsoian, A.B.; Prikhodko, V.Y.; Thomas, C.R.; Pihl, J.A.; Lardinois, T.M.; Gounder, R.; Wei, X.; Ji, Y.; et al. Effect of framework Al pairing on NO storage properties of Pd-CHA passive NO_x adsorbers. *Appl. Catal. B Environ.* **2023**, *322*, 122074. [[CrossRef](#)]
20. Li, Y.; Chen, D.; Xu, X.; Wang, X.; Kang, R.; Fu, M.; Guo, Y.; Chen, P.; Li, Y.; Ye, D. Cold-Start NO(x) Mitigation by Passive Adsorption Using Pd-Exchanged Zeolites: From Material Design to Mechanism Understanding and System Integration. *Environ. Sci. Technol.* **2023**, *57*, 3467–3485. [[CrossRef](#)]
21. Huang, S.; Wang, Q.; Shan, Y.; Shi, X.; Liu, Z.; He, H. Effects of Si/Al Ratio on Passive NO_x Adsorption Performance over Pd/Beta Zeolites. *Molecules* **2023**, *28*, 3501. [[CrossRef](#)]
22. Treacy, M.M.J.; Higgins, J.B. *Collection of Simulated XRD Powder Patterns for Zeolites*, 5th ed.; Elsevier: Amsterdam, The Netherlands, 2007.
23. Matarrese, R.; Castoldi, L.; Morandi, S.; Ticali, P.; Valsania, M.C.; Lietti, L. NO adsorption/desorption pathways over Pd/SSZ-13 low temperature NO_x adsorbers investigated by operando FT-IR spectroscopy and microreactor study. *Appl. Catal. B* **2023**, *331*, 122723. [[CrossRef](#)]
24. Khivantsev, K.; Jaegers, N.R.; Koleva, I.Z.; Aleksandrov, H.A.; Kovarik, L.; Engelhard, M.; Gao, F.; Wang, Y.; Vayssilov, G.N.; Szanyi, J. Stabilization of Super Electrophilic Pd⁺² Cations in Small-Pore SSZ-13 Zeolite. *J. Phys. Chem. C* **2020**, *124*, 309–321. [[CrossRef](#)]
25. Hadjiivanov, K.I.; Vayssilov, G.N. Characterization of oxide surfaces and zeolites by carbon monoxide as an IR probe molecule. *Adv. Catal.* **2002**, *47*, 307–511.
26. Aylor, A.W.; Lobree, L.J.; Reimer, J.A.; Bell, A.T. Investigations of the Dispersion of Pd in H-ZSM-5. *J. Catal.* **1997**, *172*, 453–462. [[CrossRef](#)]
27. Onida, B.; Geobaldo, F.; Testa, F.; Crea, F.; Garrone, E. FTIR investigation of the interaction at 77 K of diatomic molecular probes on MCM-22 zeolite. *Micropor. Mesopor. Mat.* **1999**, *30*, 119–127. [[CrossRef](#)]
28. Khivantsev, K.; Jaegers, N.R.; Kovarik, L.; Hanson, J.C.; Tao, F.F.; Tang, Y.; Zhang, X.; Koleva, I.Z.; Aleksandrov, H.A.; Vayssilov, G.N.; et al. Achieving Atomic Dispersion of Highly Loaded Transition Metals in Small-Pore Zeolite SSZ-13: High-Capacity and High-Efficiency Low-Temperature CO and Passive NO_x Adsorbers. *Angew. Chem. Int. Ed. Engl.* **2018**, *57*, 16672–16677. [[CrossRef](#)]
29. Mandal, K.; Gu, Y.; Westendorff, K.S.; Li, S.; Pihl, J.A.; Grabow, L.C.; Epling, W.S.; Paolucci, C. Condition-Dependent Pd Speciation and NO Adsorption in Pd/Zeolites. *ACS Catal.* **2020**, *10*, 12801–12818. [[CrossRef](#)]
30. Khivantsev, K.; Gao, F.; Kovarik, L.; Wang, Y.; Szanyi, J. Molecular Level Understanding of How Oxygen and Carbon Monoxide Improve NO_x Storage in Palladium/SSZ-13 Passive NO_x Adsorbers: The Role of NO⁺ and Pd(II)(CO)(NO) Species. *J. Phys. Chem. C* **2018**, *122*, 10820–10827. [[CrossRef](#)]

31. Chakarova, K.; Ivanova, E.; Hadjiivanov, K.; Klissurski, D.; Knözinger, H. Co-ordination chemistry of palladium cations in Pd-H-ZSM-5 as revealed by FTIR spectra of adsorbed and co-adsorbed probe molecules (CO and NO). *Phys. Chem. Chem. Phys.* **2004**, *006*, 3702–3709. [[CrossRef](#)]
32. Kim, P.; Van der Mynsbrugge, J.; Aljama, H.; Lardinois, T.M.; Gounder, R.; Head-Gordon, M.; Bell, A.T. Investigation of the Modes of NO Adsorption in Pd/H-CHA. *Appl. Catal. B Environ.* **2022**, *304*, 120992. [[CrossRef](#)]
33. Hadjiivanov, K.I. Identification of Neutral and Charged N_xO_y Surface Species by IR Spectroscopy. *Catal. Rev.* **2000**, *42*, 71–144. [[CrossRef](#)]
34. Hadjiivanov, K.; Saussey, J.; Freysz, J.L.; Lavalley, J.C. FT-IR study of NO+O₂ co-adsorption on H-ZSM-5: Re-assignment of the 2133 cm⁻¹ band to NO⁺ species. *Catal. Lett.* **1998**, *52*, 103–108. [[CrossRef](#)]
35. Vos, A.M.; Mignon, P.; Geerlings, P.; Thibault-Starzyk, F.; Schoonheydt, R.A. Probing the basicity of zeolite frameworks with N₂O₄: A DFT approach. *Micropor. Mesopor. Mat.* **2006**, *90*, 370–376. [[CrossRef](#)]
36. Szanyi, J.; Hun Kwak, J.; Moline, R.A.; Peden, C.H.F. The adsorption of NO₂ and the NO + O₂ reaction on Na-Y, FAU: An in situ FTIR investigation. *Phys. Chem. Chem. Phys.* **2003**, *5*, 4045–4051. [[CrossRef](#)]
37. Perdana, I.; Creaser, D.; Öhrman, O.; Hedlund, J. A comparison of NO_x adsorption on Na, H and BaZSM-5 films. *Appl. Catal. B Environ.* **2007**, *72*, 82–91. [[CrossRef](#)]
38. Khivantsev, K.; Jaegers, N.R.; Kovarik, L.; Prodinge, S.; Derewinski, M.A.; Wang, Y.; Gao, F.; Szanyi, J. Palladium/Beta zeolite passive NO_x adsorbers (PNA): Clarification of PNA chemistry and the effects of CO and zeolite crystallite size on PNA performance. *Appl. Catal. A Gen.* **2019**, *569*, 141–148. [[CrossRef](#)]
39. Gupta, A.; Kang, S.B.; Harold, M.P. NO_x uptake and release on Pd/SSZ-13: Impact of feed composition and temperature. *Catal. Today* **2021**, *360*, 411–425. [[CrossRef](#)]
40. Villamaina, R.; Iacobone, U.; Nova, I.; Tronconi, E.; Ruggeri, M.P.; Mantarosie, L.; Collier, J.; Thompsett, D. Mechanistic insight in NO trapping on Pd/Chabazite systems for the low-temperature NO_x removal from Diesel exhausts. *Appl. Catal. B Environ.* **2021**, *284*, 119724. [[CrossRef](#)]
41. Mei, D.; Gao, F.; Szanyi, J.; Wang, Y. Mechanistic insight into the passive NO_x adsorption in the highly dispersed Pd/HBEA zeolite. *Appl. Catal. A Gen.* **2019**, *569*, 181–189. [[CrossRef](#)]
42. Castoldi, L.; Matarrese, R.; Morandi, S.; Ticali, P.; Lietti, L. Low-temperature Pd/FER NO_x adsorbers: Operando FT-IR spectroscopy and performance analysis. *Catal. Today* **2021**, *360*, 317–325. [[CrossRef](#)]

Disclaimer/Publisher's Note: The statements, opinions and data contained in all publications are solely those of the individual author(s) and contributor(s) and not of MDPI and/or the editor(s). MDPI and/or the editor(s) disclaim responsibility for any injury to people or property resulting from any ideas, methods, instructions or products referred to in the content.